ACS OMEGA

Article

Cite This: ACS Omega 2018, 3, 15361−15369

http://pubs.acs.org/journal/acsodf

Transprotein-Electropore Characterization: A Molecular Dynamics Investigation on Human AQP4

Paolo Marracino,*[,†] Mario Bernardi,[†] Micaela Liberti,*[,†] Federico Del Signore,[†] Erika Trapani,[†,∥] José-Antonio Gárate,[‡] Christian J. Burnham,[§] Francesca Apollonio,*[,†] and Niall J. English*[,§]

[†]Department of Information Engineering, Electronics and Telecommunications, La Sapienza University, 00184 Rome, Italy

[‡]Centro Interdisciplinario de neurociencia de Valparaiso, Universidad de Valparaiso, 05101 Valparaiso, Chile

[§]School of Chemical and Bioprocess Engineering, University College Dublin, Belfield, D4 Dublin, Ireland

ABSTRACT: Electroporation characterization is a topic of intensive interest probed by extensive ongoing research efforts. Usually, these studies are carried out on lipid-bilayer electroporation. Surprisingly, the possibility of water-channel electropore formation across transmembrane proteins themselves, particularly in view of such a promising application, has not yet been elucidated. The present work examines the geometrical and kinetic aspects of electropores and their stability in such a protein milieux (as opposed through the phospholipid membranes) in depth, by means of scrutiny of such a process in human-AQP4 as a well-representative prototype. The residues forming the electropore's walls, organized in loops, reveal the formation mechanism by their dipole alignment and translational response in response to applied axial electric fields in nonequilibrium molecular dynamics simulation. The magnitude of sustaining electric fields (keeping a stable electropore open) were determined. This suggests that transmembrane proteins could play a central role in electroporation applications, e.g., in medicine and biotechnology.

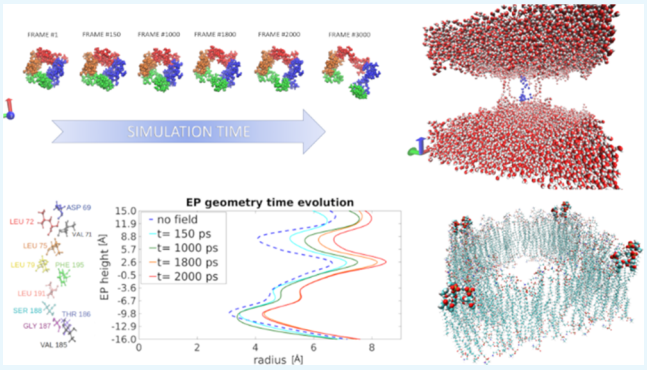

INTRODUCTION

The membrane phospholipid bilayer can be studied as a thin isolating sheet dividing two electrolyte solutions and enveloping intracellular components and organelles.[1] If this structure is exposed to an electric field pulse able to induce a transmembrane potential above a certain threshold value, the cell membrane will be permeabilized.[2] Depending on the duration of the pulse and the field intensity, the two systems on either side of the bilayer will no longer be isolated if electroporation through the membrane occurs, and molecules that could not flow through the transport-selective endogenous channels in bilayer-embedded proteins are then allowed to permeate through the electroporated membrane.[3] The transiently reversible opening of the cell enables drugs and oligonucleotides to be transported, in addition to, inter alia, antibodies, permitting the initiation of biological events by changing the inside of the cell.[4]

The mechanistic detail of how pores form under the action of applied electric fields is inherently challenging to be elucidated by experiments; conversely, this is entirely possible to explore using carefully conducted molecular dynamics (MD) simulation due to the very short time scales of the pore-formation process and also the small space scale of lipid pores (a few nanometers).[5] According to MD simulations of lipid bilayers, nanometer-sized aqueous pores are formed inside the lipid bilayers during the pulse application[6] and the kinetics of the opening and closure of these pores appear to be on the order of nanoseconds.[7] However, this description is not completely satisfactory, since it does not take into consideration, for instance, that ultrashort pulses with a very high amplitude (tens of kV/cm) and duration of a few nanoseconds, called nanopulses, have displayed long-term effects on membrane permeability and conductivity of cells and tissues, most probably due to oxidation of the membrane phospholipids induced by the field.[8]

Even if not yet fully demonstrated, another option of long-lasting (electropore) permeability due to nanopulses could be related to the involvement of transmembrane proteins when cells are exposed to such short and intense electric fields. Recent in vitro studies have considered the possibility that nanopulses could influence specific ion channel behavior as voltage-gated ion channels in bovine chromaffin cells,[9] whereas in a separate study, it has been proven that the calcium increase induced by ultrashort pulsed electric fields was mediated by voltage-gated calcium channels.[10] Further evidence of specific involvement of voltage-sensitive ion channels has been presented in ref 11, whereas activation of

Received: August 30, 2018
Accepted: October 22, 2018
Published: November 13, 2018

DOI: 10.1021/acsomega.8b02230
ACS Omega 2018, 3, 15361−15369

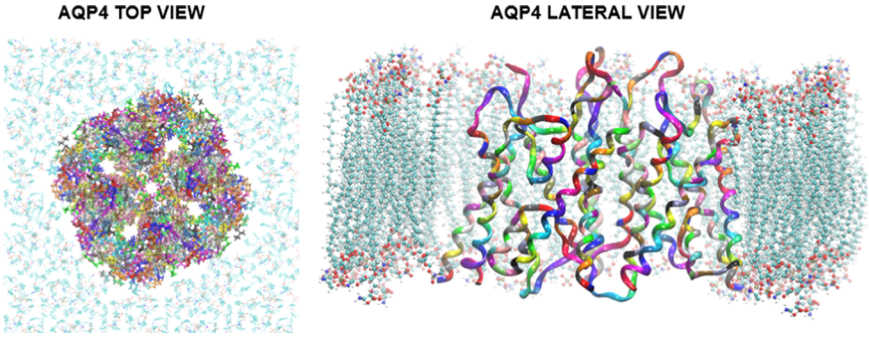

Figure 1. Left: top view (downwards, essentially along the laboratory z-axis) of the h-AQP4 embedded in the membrane (showing a fifth pore, the electropore in the middle of the four established, endogenous channels); right: lateral view, along the laboratory $x-z$ planar direction.

membrane protein modulated directly by Ca^{2+} has been shown in ref 12.

As a whole indeed, a rather tantalizing, and as-yet elusive, prospect coming from this exciting suggestion concerns the idea of controlling a drug-release course, e.g., exploiting liposomes as carriers. A potentially promising lead for achieving such a desired effect lies in aquaporins (AQPs) as prototypical water-conducting transmembrane proteins.[13,14]

In general, AQP proteins form water-conducting channels. It is interesting to observe that because of external agents,[15] human-AQP4 may undergo inner structural changes as well. According to X-ray analysis,[16] it has been observed how water flow might diminish due to narrow constrictions at the cytoplasm end. Indeed, MD computations have highlighted this mechanistically, showing the translation of a histidine[17] residue obstructing water passage.

In mammals, there are up to 11 different AQPs,[18] each one with a different role and location; however, they can be found in erythrocytes as well as in glands responsible for water secretion of saliva and sweat. A crucial role is also played in urea production and water retention in kidneys;[19] in humans, genetically defective AQPs lead to several diseases, including a rare form of diabetes[20] and polyurea. An important human aquaporin is h-AQP4,[21] a transmembrane protein that faces both the cytoplasmic and the extracellular environment as shown in Figure 1. Under physiological conditions, only four endogenous channels can be observed, but an intense driving force can induce the presence of a fifth pore. The latter creates as really small, or "finger-sized", pore at early stages and then becomes more stable.

This tetramer is embedded in the lipid bilayer and it is possible to refer to the top and bottom ends of these four different channels. If this protein is mutated though, two kinds of main problems can arise—deafness[22] and cerebral edema.[23] The few molecules that interact with aquaporin are usually toxic and subjected to strict selectivity criteria due to h-AQP4 configurations. A two-stage mechanism filter generally takes place.[24] In the middle of the channel, the first filter, made of two NPA motifs,[16,25] is observed; ions' permeability is impeded because of the activation of a strong electrical barrier. Besides this early mechanism, which can be described crudely, but effectively, by the presence of micro-dipoles,[26] there is another filter—the eponymous selectivity filter.[16] This spatially selective filter controls and modulates the passage of water, in addition to certain other solutes.

The present study focuses on the molecular mechanism of pore formation by external intense electric fields, in a particular AQP family, i.e., human AQP4, as it plays a key role in water homeostasis.[27] In particular, a principal aim of this work lies in elucidating the role of transmembrane proteins (specifically h-AQP4) in the kinetics of electropore formation. Here, the use of nonequilibrium molecular dynamics (NEMD) allows the study of the formation of electropores, both by the dipolar-orientation and translational response of residues in the AQP4 lining both endogenous channels and electropores, and by geometrical visualization and characterization of the electropores.[28]

As will be shown later, the electropore is typically created in the protein itself prior to its establishment across the membrane. Indeed, to observe the creation of a stable electropore, it is necessary, ipso facto, to work under extreme field-intensity conditions, because of the limited accessible molecular-simulation time spans of nonequilibrium molecular dynamics (NEMD) in externally applied electric fields, as has been illustrated vividly for lipid-bilayer electroporation studies;[29,30] a sufficient field strength to induce electroporation is of hundreds of megavolts per meter.[29,31] With an intense applied electric field, the large "activation energy" required to initiate pore formation can be overcome in a reasonable time window (<100 ns).[32,33] Under these circumstances, the pore formation process can be easily followed, but the pore expands to the size of the simulated bilayer patch (<100 nm^2 in most all-atom MD simulations of phospholipid bilayers), and strong finite-size effects appear. From NEMD, the molecular mechanism of electroporation has been unveiled,[5,30,32] at least for phospholipid bilayers, and the different stages of pore formation have been characterized.[34] At the same time, recent studies have also unveiled the role of an intense electric field in inducing protein structural transitions or denaturation pathways also including the role of water.[35−38]

In any event, in the present study, the simulated system is strikingly different from the earlier systems analyzed in the literature, since no transmembrane protein has been reported in any MD-based study of hydrophilic electropores. The first intriguing queries are about which domain is the first affected by the (high-intensity) porating field? Is the field inducing protein destructuring or just lipids' rearrangements? Can we observe water-channels creation within the protein core (given that the four endogenous pores remain active) or do they appear only within the lipid double layer? Indeed, in further mechanistic detail, sustaining a stable electropore is not trivial, although different lower intensities, compared with the main pore-formation field, have been investigated (vide infra). It turns out that a sustaining electric field works in this respect as long as the main field has been applied for at least one whole nanosecond according to the simulation carried out here;

DOI: 10.1021/acsomega.8b02230
ACS Omega 2018, 3, 15361−15369

otherwise, resealing occurs. The effect of these two different fields can be unveiled by studying the transient temporal behavior of these residues' dipole response to the applied field, and those defined as the most significant, especially considering their role in permeability shifts. It is well known how endogenous AQP4 channels have a bottom and a top filter, whereas in a putative fifth electropore, the most significant permeability-promoting residues would be suspected to be those adjoining the pore wall. Indeed, tackling these foregoing open questions and considerations constitute a powerful motivation for us to study electroporation in transmembrane proteins.

RESULTS

Electropore Formation. A priming NEMD simulation in the presence of a high-intensity porating field was run; more specifically, a uniform electric field was applied along the positive and negative *z*-axes for 5 ns. By visual inspection, we analyzed the NEMD trajectory, and observed the electropore creation times. As apparent from the intraprotein electropore is formed before the intramembrane electropore, coupled with a strong rearrangements of protein central residues (vide infra). This latter kind of electropore appears slowly divergent in size, compared with intraprotein electropores, quickly leading the membrane patch to irreversible expansion, borne of outright mechanical instability. Figure 2 depicts the intraprotein electropore appearance for the simulation. The water molecules penetrating the protein core are shown in blue to highlight their position, perfectly central, with respect to the four h-AQP4 endogenous pores.

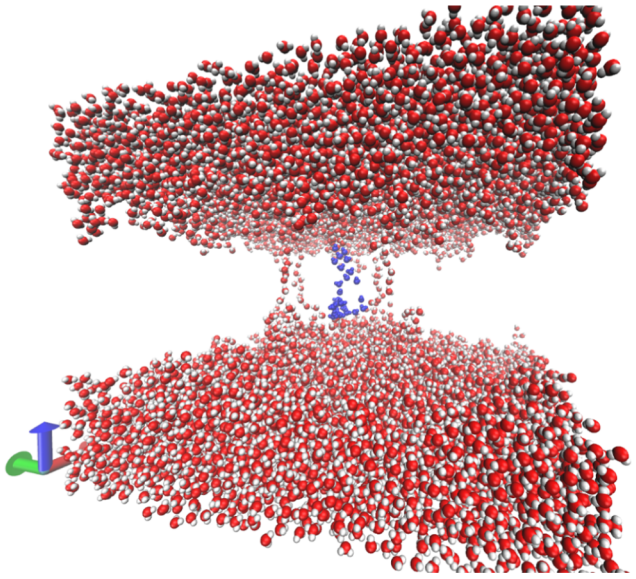

Figure 2. Water molecules within the simulated system taken at t = 150 ps; ions, lipids, and protein residues are not shown to enhance the visualization of the central intraprotein electropore (in blue).

For both intraprotein and intramembrane electropores, this limitation is an obstacle to the study of the properties and behavior of long-lasting, quasi-stable pores that are believed to exist in living, electroporated cell membranes on the basis of experimental evidence, including ion conductance.[39] It is worth noting at this point that the latter experimental evidence does not elucidate the underlying nature of such putative electropores, i.e., whether the water channel is created between the two membrane leaflets or through transmembrane proteins.

Following the methodology proposed by Fernández and coworkers,[40] consisting of a two-step protocol based on the observation that the electropores formed in MD simulations can be stabilized by reducing the applied electric field from a higher porating value to a range of lower stabilizing values, one can obtain an equilibrium condition for the electropore and thus characterize its properties with statistical soundness. We did so, which evinced structural (meta-)stability; vide infra.

Electropore Characterization. In the first 5 ns of the simulation, as shown in Figure 3, a widening actually occurs, but over 4 ns mechanical disruption is observed. This latter disruption is an irreversible electroporation event, in that it is permanent, and the study of water flux through this was not undertaken. This is the main reason why, immediately after the formation of an electropore, a lower sustaining external field should be applied; we found that up to ∼0.02 V/Å applied along the +*z*-axis could work well in this respect. Several different behaviors, occurring in particular residues, play a key role in electropore formation and in shaping them. Considering the pore as made of two halves, top and bottom, the residues can be listed systematically. Starting from the very first residue in the top half, one has ASP 69, LEU 72, VAL 71, LEU75, LEU 79; the bottom half consists of PHE 195, LEU 191, SER 188, GLY 187, THR 186, VAL 185. Each of the 11 residues of the electropore is nested in a different wall: hence, each is present four times, with each wall of the electropore originating from one of the four different endogenous h-AQP4 channels.

We plot in Figure 4 the evolution of the intraprotein radius section along the channel (cf. Materials and Methods). Here, a complete profile of the pore radius along the length of the electropore is provided. It is possible to observe, especially in the top half, an increasing effect of the electric field with the simulation time, hence providing a clear picture of the pore dynamics. Corresponding to ASP 69, VAL 71, LEU 72, and LEU 75, the first effect, small but highly relevant, is noticed at 150 ps: a variation of 0.3 Å with respect to the physiological (i.e., the unexposed simulation condition) loop radius of VAL 71, which seemingly triggers the beginning of the membrane poration (see Figure 2). Note that for the initial structure, the radius calculations suggest the presence of a sort of central endogenous channel that is too narrow for water permeation. After 1800 ps, considered as the time needed to obtain a well-formed electropore configuration, the transmembrane pore radius has widened by about 1.3 Å compared with the initial structure (cf. Figure 4). This very configuration is considered to be the one used to define a well-formed pore.[31] Such a result is legitimized by the rough structural transition of the pore, which occurs just after this time frame. Corresponding to LEU 72, a variation of 0.5 Å is computed just between 1.8 and 2 ns, indicating that an irreversible expansion of the intraprotein electropore has taken place.

Pore Quasi-Stability Achieved by a Sustaining Field. Once the electropore is created, it is necessary to act on a maintaining field to avoid both resealing and mechanical disruption. As mentioned previously, the field strength adopted, exerted along the +*z*-axis, is 0.05 V/Å. Different subsequent trajectories, primed with starting points from this simulation (mostly from 1 to 2 ns, from overall-shape considerations of Figure 4), have been run with various lower external-field intensities. Priming "sustaining-field"

DOI: 10.1021/acsomega.8b02230
ACS Omega 2018, 3, 15361−15369

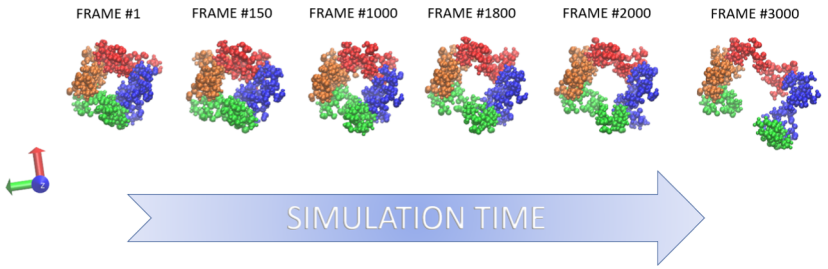

Figure 3. Evolution of the pore as seen from "above" along the laboratory z-axis is followed, with one "frame" sampled each picosecond from the instance of external-field exposure. Widening, leading to mechanical disruption, is readily evident starting from 1800 ps.

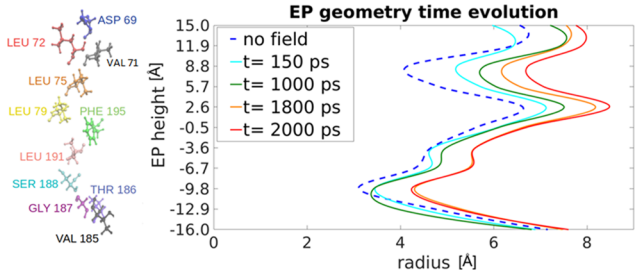

Figure 4. Evolution of the electropore's shape during the priming simulation, with one frame sampled each picosecond from the instance of external-field exposure. The most stable shape is observed between 1 and 2 ns following field exposure, during which the bulk of simulations was conducted in sustaining electric fields with different starting points from simulation #1 (vide infra).

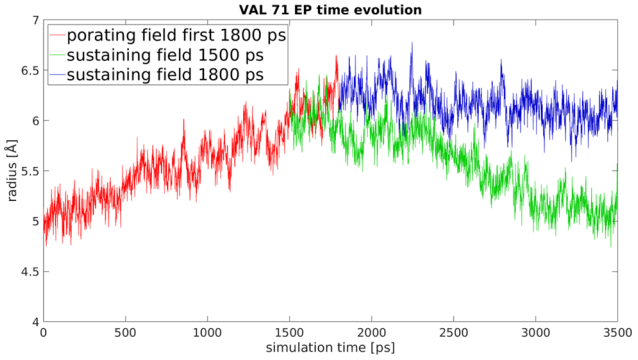

Figure 5. Time evolution of the electropore, studied from the perspective of VAL 71. On the left side is portrayed the effect of the poration field within the first 1300 ps; on the right hand is shown the effect of a sustaining field E = 0.02 V/Å applied right after the porating field has been enforced for 1300 ps. It is necessary to wait longer to avoid resealing.

simulations from the first 150−500 ps of simulation #1 leads to the electropore's fast resealing (data not shown). Moving further in time in simulation #1, the water load through the electropore increases and, eventually, up to 1 ns, a larger pore is observed; but that reseals too when the system is subjected to a lower-intensity field. In any event, in these subsequent, lower-field simulations, the sustaining field strengths investigated were 0, 0.005, 0.0075, 0.01, 0.015, and 0.02 V/Å.

Simulations starting from 1.3 to 1.5 ns, around 20 ns long, have shown resealing of pores as long as the maintaining intensity was lower than 0.02 V/Å. Visual inspection via the visual molecular dynamics (VMD) program reveals that, even if the resealing has not (yet) happened over ∼20 ns, the stable pore is small and reducing gradually in radius, albeit not quite yet finger-sized (cf. Figure 2). On the other hand, if the sustaining field is applied after 2 ns from the priming simulation, one of the endogenous channels seems to be compromised by the electropore enlargement. After 1.9 ns, the sustaining field of 0.02 V/Å induces a quasi-stable electropore, but a prominent "touching" contact between it and one of the endogenous channels becomes persistent after ∼35 ns. After extensive, careful checking and visualization, a large, quasi-stable electropore is maintained by a 0.02 V/Å field, over up to ∼50 ns from which simulations were run for starting points at 1.6, 1.7, and 1.8 ns from the porating field simulation. Figure 5 shows the time evolution of the transprotein electropore radius, studied from the perspective of four VAL 71 residues' loop, during the porating field application (red curve) and in two different sustaining field scenarios: (i) the first one referred to a well-formed pore at 1500 ps (green curve); (ii) the second one referred to a well-formed pore at 1800 ps (blue curve). Although, at first glance, similar by simple visual inspection, the two starting configurations at 1500 and 1800 ps lead to completely different electropore dynamics, as apparent from the figure.

The main objective of this section lies in the analysis of the transprotein electropore quasi-stable dynamics when the electric sustaining field is applied after 1800 ps from the porating field simulation, given the intrinsic stability of the pore geometry within 1500 ps. The field effect on the transprotein structural rearrangements can be soundly linked to the coupling with the intrinsic dipoles of protein residues' dipoles. In particular, we focused on the top-half single residues. Each residue has been analyzed, computing the dipole moment with respect to its center of mass, but only the most interesting residues, according to the magnitude of the coupling with the electric field, have been studied thoroughly. Hence, in Figure 6, the probability distribution of the z-component (the same direction of the exogenous applied field) of the dipole moment corresponding to the very top protein residue, ASP 69, is portrayed. To appreciate the coupling effect of the exogenous field with such dipoles, we considered three different cases: (i) physiological conditions, represented by a 10 ns equilibrium simulation (i.e., no field is applied); (ii) the application of the 0.05 V/Å porating field until 1800 ps; (iii) the application of a 0.02 V/Å sustaining field, starting from a well-formed transprotein electropore configuration. In the figure, it is possible to outline, under physiological conditions, two different dipolar states, only barely hinted in the second protein monomer (B). The conclusion to be drawn from this kind of observation is related to the occurrence of an angular flip of the dipole associated with the residue. During the poration-field application, this flip does not occur at all, and the dipole populates only one of the two states initially

DOI: 10.1021/acsomega.8b02230
ACS Omega 2018, 3, 15361−15369

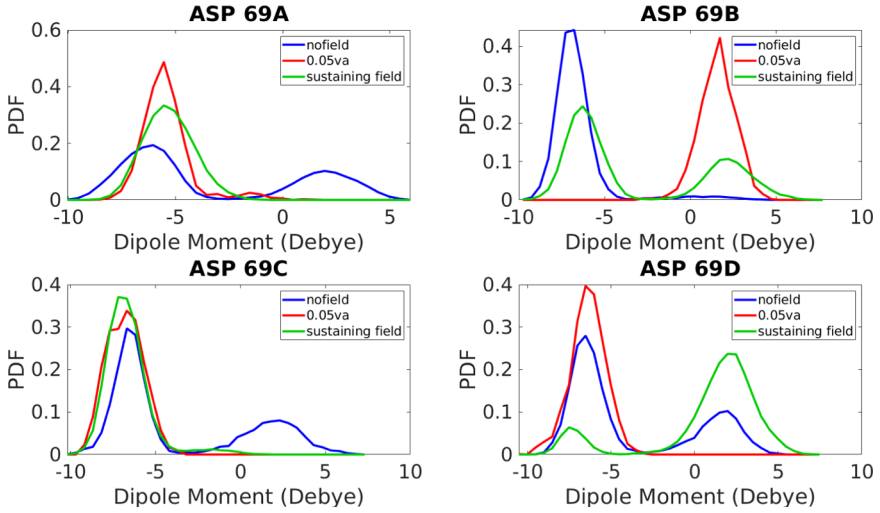

Figure 6. ASP 69 probability distribution functions of the z component of the dipolar moment in each of the four walls. The plots represent (i), (ii), and (iii) situations depicted as blue, red, and light green curves, respectively.

available. When the sustaining field is applied, it is possible to notice a partial return to the initial pre-exposition condition, although in ASP 69A and ASP 69C (protein first and third monomers), the dipole polarization seems to be still irreversible, at least during the simulation duration (20 ns).

DISCUSSION

In the present contribution, many aspects of pore formation in transmembrane proteins have been discussed. If one correlates the pore formation event with a strong dipolar coupling with the exogenous electric field, we verified in Figure 6, a clear shift of the ASP 69 residue dipole moment in correspondence to the porating field application. This event matches with the disappearance of one of the two accessible ASP 69 dipolar states appreciated in the unexposed simulation. To verify the connection of this result with the location of electropore appearance, which seems more frequent within the transmembrane protein than in the membrane, ASP 69 was chosen as a representative of the membrane dipolar coupling with the field. Figure 7a represents the probability distribution of the z-component of the 12 lipid heads dipole (lipid cores are neutral, see Figure 7b). As shown in Figure 7b, the lipid heads have been drawn from the corner of the box, since it was desired to make the calculation as close as possible to bulk conditions, exploiting periodic boundary conditions. A significant effect, equivalent or stronger compared with that of ASP 69 residues, due to the porating field is observed. Nevertheless, looking at the unexposed simulation, in contrast to the results shown in Figure 7a, no distinguishable dipolar states are present. The effect of the porating field, although clear, is partially hidden by the wide probability distribution profile, making less immediate the relation between dipole rotations and water molecules' protrusion into the membrane.

Figure 3 shows how after a main field is applied, sustaining the electropore is of paramount importance to avoid mechanical disruption. When enforcing a strong static electric field, such as $E = 0.05$ V/Å, time and sustaining field intensities have been studied thoroughly. The aim, after witnessing water-finger formation and the birth of a small pore, is of maintaining a large stable one. It turns out, as hinted in Figure 5, that it is not possible to sustain a (quasi-)stable electropore when moving out of the time interval 1−2 ns. The pore either reseals

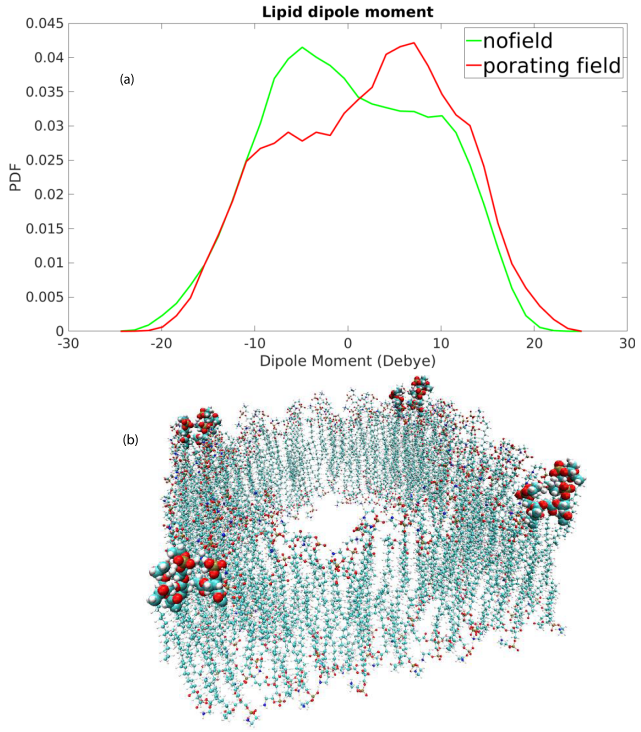

Figure 7. (a) Upper: probability distribution function of the lipid's dipole moments; the red curve is characteristic of the unexposed case, whereas the light green curve shows the shift relative to the dipolar moment when the porating field is applied. (b) Lower: the lipid dipole moments shown in panel (a) are averaged over 12 lipid heads, close to the corner of the system, as visualized in VMD; indeed, it is possible to observe the polar heads of the lipids in the upper leaflet, highlighted as they represent the only charged moieties within the lipid structure.

within the first 10 ns or diverges, tending to devour one of the endogenous channels. The only intensity suitable, and reliable, for this task appeared to be 0.02 V/Å. In fact, for sustaining fields applied after 1.6, 1.7, or 1.8 ns of 0.05 V/Å-field exposure, the electropore was stable for 20 ns-long runs, and longer still. Such stable pores have been characterized in terms of geometry and dipolar mechanism. Under these circum-

DOI: 10.1021/acsomega.8b02230
ACS Omega 2018, 3, 15361−15369

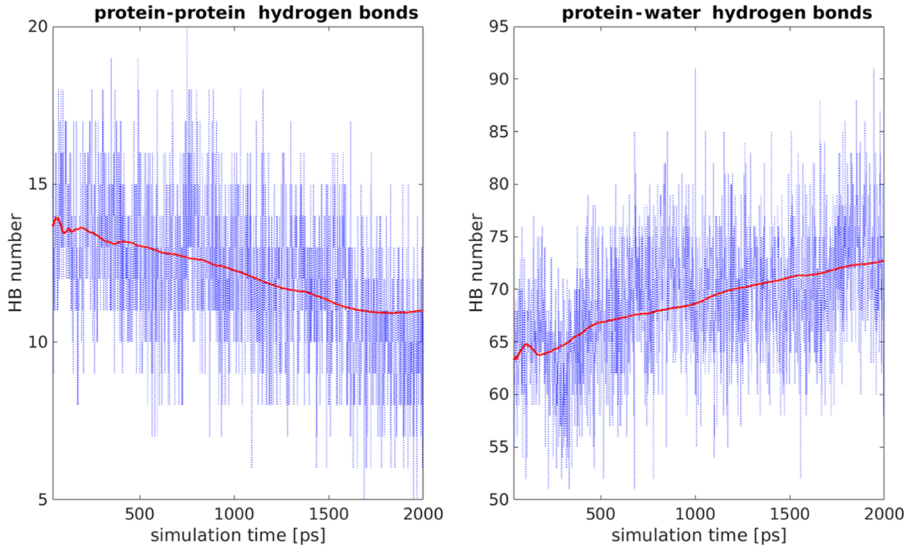

Figure 8. Effect of the porating field (E = 0.05 V/Å) on the number of hydrogen bonds in the electropore region in the first 2000 ps, before mechanical disruption takes place. On the left-hand side, the HB number within the protein is reported, whereas on the right-hand side, the HB number stemming from the interaction of water molecules with the protein is reported. Red curves represent data smoothed with a moving average filter with a 30% span.

stances, ionic conductivity events have been recorded and will be explored further thoroughly in a future publication.

The variation of permeability can be possibly linked to the number of hydrogen bonds (HB) within the electropore. This analysis was carried on in the VMD setting of an acceptor−donor (O···O) distance of 3.5 Å along with an angle (H−O···O) smaller than 30°. These parameters were selected according to the standard set by Farimani et al.,[41] although they do not mimic the precise hydrogen-bond conditions of ref 41. In their pioneering work,[41] based on CNTs, the enhancement of permeability was a consequence of a decrease in the number of hydrogen bonds over the peripheral regions of the CNT wall, since the number of hydrogen bonds essentially determines the degrees of freedom for water molecules. On the basis of this well-known geometrical effect, we decided to relate the number of hydrogen bonds during the application of a 0.05 V/Å porating field to the electropore's structural transition reported in Figure 4. The dynamics of the hydrogen bonds within the residues surrounding the electropore and between such residues and water molecules within the electropore were both investigated. It is apparent from Figure 8 that within the time interval representative of electropore expansion, the number of protein−protein hydrogen bonds decreases in a monotonic fashion (only for protein residues identified in the previous section), reaching a plateau region after 1700 ps, where a 0.02 V/Å electric field is sufficient to sustain a stable electropore. When considering the number of protein−water hydrogen bonds, on the other hand, the opposite behavior is observed, which can be related to the enlargement of the water channel within the electropore. It is worth noting that the percentage variation in the number of hydrogen bonds is much larger within the selected protein residues, indicative of a strong interaction with the exogenous electric field.

CONCLUSIONS

The physical mechanisms underlying the interaction of electric pulses and cell membranes have not been fully elucidated, in particular, concerning the involvement and specific role of transmembrane proteins. Molecular dynamics simulations has proven to be a valid tool for the investigation of such interactions also due to the difficulties in performing experiments on such nanometer scales.

Here, we have scrutinized geometric and kinetic aspects of transmembrane electroporation and assessed their resultant underlying stability. Mechanistic analysis of electropore wall dipole alignment reveals the subtle interplay of, and dependence on, translational and rotational response in response to axially applied electric fields. In particular, the ASP 69 residue (overlooking the extracellular medium) exhibits two accessible states upon field exposure, and when the field is enforced, only one holds, whereas the lipid heads show no transition from one state to the other. This signifies, we conjecture, the lower propensity of lipids to reorganize in the case of the embedded h-AQP4 to reorganize to allow electropore formation therein, displaying faster underlying dynamics than standard lipid electropores. In addition, we must emphasize the key role of hydrogen bonds in terms of breaking and reformation in applied fields as of paramount importance in determining the details of electroporation subsequent stability, mediated by dipole rotational and transitional field response. Indeed, the occasional observation of ionic-conductivity events through the electropore (not discussed here) is an interesting phenomenon, which we intend to study further.

With the very recent and exciting advent of high-quality, large-field experimental studies on electroporation, showing reversible electropermeabilization,[42,43] and more general studies on protein structure and function manipulation (reaching up to the 0.01 V/Å range),[44] the importance of NEMD simulation as an accompanying tool for hand-in-glove progress with electric-field experiments is to be noted.

MATERIALS AND METHODS

Molecular Modelling. The trajectories are simulated making use of NAMD v2.9[45,46] starting from an h-AQP4 Protein Data Bank[47] entry 3GD8 file. This configuration is open to different protonation states. Keeping this in mind, hydrogen atoms were added, in the CHARMM27 topology

DOI: 10.1021/acsomega.8b02230
ACS Omega 2018, 3, 15361−15369

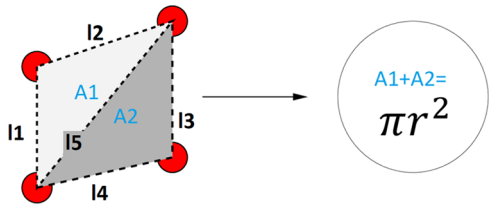

Figure 9. Pores are made of 11 loops, each one consisting of a repetition of four identical residues. The centers of mass of the residues for a single loop are depicted in red here. Summing the areas of the two triangles, obtained by Heron's formula, it is possible to estimate the radius of the pore corresponding to a given loop.

internal coordinates,[48,49] to be consistent with pH 7.5. This tetramer is then embedded in a palmitoyloleoylphosphatidylethanolamine lipid bilayer, which is solvated and equilibrated. The membrane's overlapping lipids were removed and a solvation shell of 20 Å is added on the $\pm z$ axes. This entire system is made electrically neutral by the presence of Na^+ and Cl^- ions, the resulting concentration being 55 mM. The resulting periodic cell volume is 101 × 101 × 80 $Å^3$.

Molecular Dynamics Simulation. CHARMM27[49] and TIP3P[50] potential models were used. CHARMM27 is a nonpolarizable potential, in contrast to previous work of English et al.,[51−53] but returns qualitative acceptable outcomes.[54] Long-range electrostatic interactions were handled by the particle mesh Ewald method, making use of r-RESPA decomposition.[17] Each simulation relies on an NPT reservoir for coupling. The reservoir pressure and temperature point were set respectively to 1 atm and 298 K. Temperature was controlled through a Langevin thermostat with a damping coefficient of 1 ps^{-1}.[55−57] The applied electric field was static, and acted in the direction of the positive z-axis; as reported above, a strength of 0.05 V/Å led to electroporation. The static-field force was applied to atomic partial charges, using $f = qE_0$. This kind of system response of water to electric fields in nanoscale geometries embedded in phospholipid bilayers has been studied extensively by Garate and co-workers.[17,58,59,60]

Pore Profile. To obtain the cross-sectional area of the electropore, an equivalent-area method was implemented, keeping in mind that each of the 11 residues is at a slightly different "height" along the z-axes. Here, we consider a square as composed of two triangles, whose areas are computed through Heron's formula

$$A_{tr1} = \sqrt{p(p - l_1)(p - l_2)(p - l_5)}$$

$$A_{tr2} = \sqrt{p(p - l_3)(p - l_4)(p - l_5)}$$

$$A = A_{tr1} + A_{tr2} = \pi r^2$$

where A is the cross-sectional area, l_1, l_2, and l_3 are the side lengths, and p is the semiperimeter, i.e., $1/2(l_1 + l_2 + l_5)$. The radius of the circle inscribed in the square, as shown in Figure 9, provides a rough estimate of the electropore radius within a given residue loop.

AUTHOR INFORMATION

Corresponding Authors

*E-mail: marracino@diet.uniroma1.it. Tel: +39-06-4458-5457 (P.M.).

*E-mail: micaela.liberti@uniroma1.it. Tel: +39-06-4458-5353 (M.L.).

*E-mail: francesca.apollonio@uniroma1.it. Tel: +39-06-4458-5374 (F.A.).

*E-mail: niall.english@ucd.ie. Tel: +353-1-716-1646. Fax: +353-1-716-1177 (N.J.E.).

ORCID

Niall J. English: 0000-0002-8460-3540

Present Address

‖Accenture Consulting, Piazzale dell'industria, 40, 00144 Rome, Italy (E.T.).

Notes

The authors declare no competing financial interest.

ACKNOWLEDGMENTS

The authors thank Zdenek Futera, Mohammad Reza Ghaani, and Massimiliano Avena for interesting discussions and technical assistance. J.A.G. acknowledges financial support from CM-Economía grant P09-022-F CINV and Universidad de Valparaíso, FONDECYT grant No. 1180987 and PAI grant No. 77170045. M.L. acknowledges financial support from grant No. RM11715C7DCB8473, University Sapienza of Rome and F.A. acknowledges financial support from grant No. RM116154E273BDD4 University Sapienza of Rome.

REFERENCES

(1) Van Meer, G.; Voelker, D. R.; Feigenson, G. W. Membrane lipids: where they are and how they behave. *Nat. Rev. Mol. Cell Biol.* **2008**, *9*, 112−124.

(2) (a) Schwan, H. P. *Biological Effects and Dosimetry of Nonionizing Radiation*; Springer: Boston, MA, 1983. (b) Kotnik, T.; Pucihar, G.; Miklavcic, D. Induced transmembrane voltage and its correlation with electroporation-mediated molecular transport. *J. Membr. Biol.* **2010**, *236*, 3−13.

(3) Weaver, J. C.; Chizmadzhev, Y. A. Theory of electroporation: a review. *Bioelectrochem. Bioenergy* **1996**, *41*, 135−160.

(4) Mir, L. M. Bases and rationale of the electrochemotherapy. *EJC Suppl.* **2006**, *4*, 38−44.

(5) Tarek, M. Membrane Electroporation: A Molecular Dynamics Simulation. *Biophys. J.* **2005**, *88*, 4045−4053.

(6) Tieleman, D. P. The molecular basis of electroporation. *BMC Biochem.* **2004**, *5*, No. 10.

(7) Vernier, P. T.; Levine, Z. A.; Wu, Y.-H. H.; Joubert, V.; Ziegler, M. J.; Mir, L. M.; Tieleman, D. P.; et al. Electroporating fields target oxidatively damaged areas in the cell membrane. *PLoS One* **2009**, *4*, No. e7966, DOI: 10.1371/journal.pone.0007966.

(8) Breton, M.; Mir, L. M. Investigation of the chemical mechanisms involved in the electropulsation of membranes at the molecular level. *Bioelectrochemistry* **2018**, *119*, 76−83.

(9) Craviso, G. L.; Choe, S.; Chatterjee, P.; Chatterjee, I.; Vernier, P. T. Nanosecond electric pulses: A novel stimulus for triggering Ca2+ influx into chromaffin cells via voltage-gated Ca2+ channels. *Cell. Mol. Neurobiol.* **2010**, *30*, 1259−1265.

(10) Semenov, I.; Xiao, S.; Kang, D.; Schoenbach, K. H.; Pakhomov, A. G. Cell stimulation and calcium mobilization by picosecond electric pulses. *Bioelectrochemistry* **2015**, *105*, 65−71.

(11) Burke, R. C.; Bardet, S. M.; Carr, L.; Romanenko, S.; Arnaud-Cormos, D.; Leveque, P.; O'Connor, R. P. Nanosecond pulsed electric fields depolarize transmembrane potential via voltage-gated K +, Ca2+ and TRPM8 channels in U87 glioblastoma cells. *Biochim. Biophys. Acta* **2017**, *1859*, 2040−2050.

(12) Muratori, C.; Pakhomov, A. iG.; Gianulis, E.; Meads, J.; Casciola, M.; Mollica, P. A.; Pakhomova, O. N. Activation of the phospholipid scramblase TMEM16F by nanosecond pulsed electric fields (nsPEF) facilitates its diverse cytophysiological effects. *J. Biol. Chem.* **2017**, *292*, 19381−19391.

(13) Hohmann, S.; Nielsen, S.; Agre, P. *Aquaporins*; Academic Press: San Diego, CA, 2001.

DOI: 10.1021/acsomega.8b02230
ACS Omega 2018, 3, 15361−15369

(14) Borgnia, M.; et al. Cellular and molecular biology of the aquaporin water channels. *Annu. Rev. Biochem.* **1999**, *68*, 425−458.
(15) Marracino, P.; Liberti, M.; Trapani, E.; Burnham, C.; Avena, M.; Garate, J.-A.; Apollonio, F.; English, N. J. Human Aquaporin 4 Gating Dynamics Under Perpendicularly - Oriented Electric-Field Impulses: A Molecular Dynamics Study. *Int. J. Mol. Sci.* **2016**, *17*, 1133.
(16) Ho, J. D.; Yeh, R.; Sandstrom, A.; Chorny, I.; Harries, W. E. C.; Robbins, R. A.; Miercke, L. J. W.; Stroud, R. M.; et al. Crystal structure of human aquaporin 4 at 1.8 Å and its mechanism of conductance. *Proc. Natl. Acad. Sci. U.S.A.* **2009**, *106*, 7437−7442.
(17) Reale, R.; English, N. J.; Garate, J.-A.; Marracino, P.; Liberti, M.; Apollonio, F. Human Aquaporin 4 Gating Dynamics Under and After Nanosecond-Scale Static and Alternating Electric-Field Impulses: A Molecular Dynamics Study of Field Effects and Relaxation. *J. Chem. Phys.* **2013**, *139*, No. 205101.
(18) Ishibashi, K.; Hara, S.; Kondo, S. Aquaporin water channels in mammals. *Clin. Exp. Nephrol.* **2009**, *13*, 107−117.
(19) Verkman, A. S.; Phuan, P.-W.; Asavapanumas, N.; Tradtrantip, L. Biology of AQP4 and anti-AQP4 antibody: therapeutic implications. *Brain Pathol.* **2013**, *23*, 684−695.
(20) Verkman, A. S. Aquaporins in Clinical Medicine. *Annu. Rev. Med.* **2012**, *63*, 303−316.
(21) Papadopoulos, M. C.; Verkman, A. S. Aquaporin water channels in the nervous system. *Nat. Rev. Neurosci.* **2013**, *14*, 265−277.
(22) Christensen, N.; D'Souza, M.; Zhu, X.; Frisina, R. D. Age-related hearing loss: Aquaporin 4 gene expression changes in the mouse cochlea and auditory midbrain. *Brain Res.* **2009**, *1253*, 27−34.
(23) Verkman, A. S.; Binder, D. K.; Bloch, O.; Auguste, K.; Papadopoulos, M. C. Three distinct roles of aquaporin-4 in brain function revealed by knockout mice. *Biochim. Biophys. Acta, Biomembr.* **2006**, *1758*, 1085−1093.
(24) Hub, J. S.; Aponte-Santamaria, C.; Grubmüller, H.; de Groot, B. L.; et al. Voltage-regulated water flux through aquaporin channels in silico. *Biophys. J.* **2010**, *99*, L97−L99.
(25) Törnroth-Horsefield, S.; Hedfalk, K.; Fischer, G.; Lindkvist-Petersson, K.; Neutze, R. Structural insights into eukaryotic aquaporin regulation. *FEBS Lett.* **2010**, *584*, 2580−2588.
(26) Alberga, D.; Nicolotti, O.; Lattanzi, G.; Nicchia, G. P.; Frigeri, A.; Pisani, F.; Benfenati, V.; Mangiatordi, G. F. A new gating site in human aquaporin-4: Insights from molecular dynamics simulations. *Biochim. Biophys. Acta, Biomembr.* **2014**, *1838*, 3052−3060.
(27) Badaut, J.; Lasbennes, F.; Magistretti, P. J.; Regli, L. Aquaporins in brain: distribution, physiology, and pathophysiology. *J. Cereb. Blood Flow Metab.* **2002**, *22*, 367−378.
(28) Marracino, P.; Liberti, M.; Vernier, P. T.; Apollonio, F. A statistical analytical model for hydrophilic electropore characterization: a comparison study. *RSC Adv.* **2017**, *7*, 31997.
(29) Böckmann, R. A.; de Groot, B. L.; Kakorin, S.; Neumann, E.; Grubmüller, H. Kinetics, Statistics, and Energetics of Lipid Membrane Electroporation Studied by Molecular Dynamics Simulations. *Biophys. J.* **2008**, *95*, 1837−1850.
(30) Kramar, P.; Delemotte, L.; Maček Lebar, A.; Kotulska, M.; Tarek, M.; Miklavčič, D. Molecular-level characterization of lipid membrane electroporation using linearly rising current. *J. Membr. Biol.* **2012**, *245*, 651−659.
(31) Levine, Z. A.; Vernier, P. T. Life cycle of an electropore: field-dependent and field independent steps in pore creation and annihilation. *J. Membr. Biol.* **2010**, *236*, 27−36.
(32) Tieleman, D. P. The molecular basis of electroporation. *BMC Biochem.* **2004**, *5*, No. 10.
(33) Ziegler, M. J.; Vernier, P. T. Interface water dynamics and porating electric fields for phospholipid bilayers. *J. Phys. Chem. B* **2008**, *112*, 13588−13596.
(34) Fernández, M. L.; Marshall, G.; Sagués, F.; Reigada, R. Structural and kinetic molecular dynamics study of electroporation in colesterol-containing bilayers. *J. Phys. Chem. B* **2010**, *114*, 6855−6865.
(35) Marracino, P.; Migliorati, M.; Paffi, A.; Liberti, M.; Denzi, A.; D'Inzeo, G.; Apollonio, F. Signal transduction on enzymes: The Effect of electromagnetic field stimuli on superoxide dismutase (SOD). *Conf. Proc. IEEE Eng. Med. Biol. Soc.* **2012**, 5674−5677.
(36) Marracino, P.; Vernier, P. T.; Liberti, M.; Apollonio, F. Lipid Electropore Geometry in Molecular Models. In *Handbook of Electroporation*; Springer, 2017; Vol. *1*, pp 155−170.
(37) Marracino, P.; Apollonio, F.; Liberti, M.; D'Inzeo, G.; Amadei, A. Effect of high exogenous electric pulses on protein conformation: Myoglobin as a case study. *J. Phys. Chem. B* **2013**, *117* (8), 2273−2279.
(38) Avena, M.; Marracino, P.; Liberti, M.; Apollonio, F.; English, N. J. Influence of nanosecond-pulsed electric fields on water and its subsequent relaxation: dipolar effects and debunking memory. *J. Chem. Phys.* **2015**, *142*, No. 141101.
(39) Pakhomov, A. G.; Kolb, J. F.; White, J. A.; Joshi, R. P.; Xiao, S.; Schoenbach, K. H. Longlasting plasma membrane permeabilization in mammalian cells by nanosecond pulsed electric field (nsPEF). *Bioelectromagnetics* **2007**, *28*, 655−663.
(40) Fernández, M. L.; Risk, M.; Reigada, R.; Vernier, P. T. Size-controlled nanopores in lipid membranes with stabilizing electric fields. *Biochem. Biophys. Res. Commun.* **2012**, *423*, 325−330.
(41) Farimani, A. B.; Aluru, N. R. Spatial diffusion of water in carbon nanotubes: from fickian to ballistic motion. *J. Chem. Phys. B* **2011**, *115*, 12145−12149.
(42) Silve, A.; Leray, I.; Poignard, C.; Mir, L. M. Impact of external medium conductivity on cell membrane electropermeabilization by microsecond and nanosecond electric pulses. *Sci. Rep.* **2016**, *6*, No. 19957.
(43) Kotnik, T.; Frey, W.; Sack, M.; Haberl Meglič, S.; Peterka, M.; Miklavčič, D. Electroporation-based applications in biotechnology. *Trends Biotechnol.* **2015**, *33*, 480−488.
(44) Hekstra, D. R.; White, K. I.; Socolich, M. A.; Henning, R. W.; Šrajer, V.; Ranganathan, R. Electric-field-stimulated protein mechanics. *Nature* **2016**, *540*, 400−405.
(45) Humphrey, W.; et al. VMD: visual molecular dynamics. *J. Mol. Graphics* **1996**, *14*, 33−38.
(46) Phillips, J. C.; Braun, R.; Wang, W.; Gumbart, J.; Tajkhorshid, E.; Villa, E.; Chipot, C.; Skeel, R. D.; Kalé, L.; Schulten, K. Scalable molecular dynamics with NAMD. *J. Comput. Chem.* **2005**, *26*, 1781−1802.
(47) Bernstein, F. C.; Koetzle, T.; Williams, G. J. B.; Meyer, E. F.; Brice, M. D.; Rodgers, J. R.; Kennard, O.; Shimanouchi, T.; Tasumi, M. The Protein Data Bank: a computer-based archival file for macromolecular structures. *J. Mol. Biol.* **1977**, *112*, 535−542.
(48) MacKerell, A. D.; et al. All-atom empirical potential for molecular modeling and dynamics studies of proteins. *J. Phys. Chem. B* **1998**, *102*, 3586−3616.
(49) Feller, S. E.; MacKerell, A. An improved empirical potential energy function for molecular simulations of phospholipids. *J. Phys. Chem. B* **2000**, *104*, 7510−7515.
(50) Jorgensen, W. L.; Chandrasekhar, J.; Madura, J. D.; Impey, R. W.; Klein, M. L. Comparison of simple potential functions for simulating liquid water. *J. Chem. Phys.* **1983**, *79*, 926.
(51) English, N. J.; MacElroy, J. M. D. Hydrogen bonding and molecular mobility in liquid water in external electromagnetic fields. *J. Chem. Phys.* **2003**, *119*, 11806.
(52) English, N. J. Molecular dynamics simulations of microwave effects on water using different long-range electrostatics methodologies. *Mol. Phys.* **2006**, *104*, 243−253.
(53) English, N. J. Molecular dynamics simulations of liquid water using various long-range electrostatics techniques. *Mol. Phys.* **2005**, *103*, 1945−1960.
(54) English, N. J.; MacElroy, J. M. D. Atomistic simulations of liquid water using various long-range electrostatics techniques. *Mol. Phys.* **2002**, *100*, 3753−3769.
(55) Gumbart, J.; Khalili-Araghi, F.; Sotomayor, M.; Roux, B. Constant electric field simulations of the membrane potential

DOI: 10.1021/acsomega.8b02230
ACS Omega 2018, 3, 15361−15369

illustrated with simple systems. *Biochim. Biophys. Acta, Biomembr.* **2012**, *1818*, 294−302.
(56) Martyna, G. J.; Tobias, D. J.; Klein, M. L. Constant pressure molecular dynamics algorithms. *J. Chem. Phys.* **1994**, *101*, 4177−4189.
(57) Martyna, G. J.; Tobias, D. J.; Klein, M. L. Reversible multiple time scale molecular dynamics. *J. Chem. Phys* **1992**, *97*, 1990−2001.
(58) Garate, J. A.; English, N. J.; MacElroy, J. M. Human aquaporin 4 gating dynamics in dc and ac electric fields: a molecular dynamics study. *J. Chem. Phys.* **2011**, *134*, No. 055110.
(59) Garate, J. A.; English, N. J.; MacElroy, J. M. D. Static and alternating electric field and distance-dependent effects on carbon nanotube-assisted water self-diffusion across lipid membranes. *J. Chem. Phys.* **2009**, *131*, No. 114508.
(60) Garate, J.-A.; English, N. J.; MacElroy, J. M. D. Carbon nanotube assisted water self-diffusion across lipid membranes in the absence and presence of electric fields. *Mol. Simul.* **2009**, *35*, 3−12.

DOI: 10.1021/acsomega.8b02230
ACS Omega 2018, 3, 15361−15369